Molecular-dynamics simulation of hydrogen diffusion in niobium

Yinggang Li*
Department of Chemistry and Ames Laboratory, Iowa State University, Ames, Iowa 50011

Göran Wahnström†
Department of Applied Physics, Chalmers University of Technology and Göteborg University, S-412 96 Göteborg, Sweden
(Received 31 October 1994)

Molecular-dynamics simulations of H diffusion in Nb are performed for a system consisting of 432 Nb atoms and 8 H atoms at two different temperatures: T= 450 and 580 K. For the interatomic interactions we use a description proposed by Finnis, Sinclair, and Gillan. We compare our results with quasielastic-neutron-scattering data and our model reproduces quite well both the distinct deviation from simple jump-diffusion behavior and the "anomalous" Debye-Waller factor. To reveal the details of the H motion the residence-time distribution at the stable sites (T sites) as well as the correlation character among consecutive "jumps" are evaluated. We find that the residence-time distribution is composed of two distinct contributions; one narrow component with a short residence time of the order 35 fs, and one broad component with roughly exponential decay. The narrow component corresponds to that the H atom moves rapidly among two or more sites belonging to what has been called a $4T$ configuration. The typical decay time of the broad component is found to be of the order 160 fs and 300 fs in the time intervals $60 < t < 300$ fs and $300 < t < 600$ fs, respectively, which should be compared with the mean residence time derived from the diffusion constant, $\tau_{\rm res} = a_0^2/48D_s = 324$ fs. We also find substantial contributions of second-nearest-neighboring jumps, but the division between nearest- and second-nearest-neighboring jumps is ambiguous. The diffusive and the vibrational motion of the H atom cannot be clearly separated and the time spent and the spatial excursion performed in the "jump phase" are not negligible.

I. INTRODUCTION

Hydrogen motion in bcc metals has been a subject of great interest, both experimentally and theoretically.[1,2] The main experimental tool for studying the microscopic motion of hydrogen is inelastic neutron scattering. Despite extensive experimental investigations during the last 25 years features still remain unclear for the details of the migration mechanism operating in real systems, as for instance for H in Nb above room temperature.[3]

Several different contributions of the hydrogen motion have been identified in the incoherent neutron-scattering spectrum.[1,2] At high frequencies, 100 – 200 meV, localized vibrational modes are manifest and well separated from these are the so-called band modes, visible in the range < 30 meV. These modes correspond to the fact that hydrogen follows the vibrations of the host metal atoms. Besides these vibrational contributions the spectrum contains a quasielastic peak, centered at zero frequency, which includes information on the diffusive motion. Both the integrated intensity of this peak and its shape have been investigated intensively.

Anomalies in the wave vector dependence of the integrated intensity of the quasielastic peak for H in Nb have been identified at elevated temperatures and are referred to as the anomalous Debye-Waller factor. Gissler *et al.*[4] observed a marked deviation from a simple Debye-Waller factor at high temperatures. They discussed the possibility of the importance of taking the finite jump time into account but concluded that at least a free jumping particle model for that motion could be excluded. Wakabayashi *et al.*[5] interpreted the anomalous Debye-Waller factor in terms of a temperature-dependent delocalization of the hydrogen vibrational motion extending as far as nearest-neighboring sites of the interstitial lattice. Later, Lottner *et al.*[6] made a more careful fitting procedure of the quasielastic peak using jump-diffusion models containing correlated jumps and claimed that no serious deviation from the normal Debye-Waller factor could be identified. More recently, Dosch *et al.*[3] reinvestigated the intensity and stated that a proper interpretation of the intensity has to include a rapid-diffusion mechanism, on a time scale significantly faster than conventional long-range diffusion.

The wave vector dependence of the width also shows nontrivial features. Above room temperature distinct deviations from simple jump-diffusion behavior are obtained. A double-jump model and a two-state model, with a mobile and an immobile state, respectively, have been used to successfully fit the data.[7] The physical implications are not, however, very clear. In the double-jump model the probability of a direct jump to a topological second nearest neighbor is considerably larger than a jump to a nearest neighboring site at high temperatures, and in the two-state model the mean occupancy of the mobile state is nearly temperature independent, which challenges the interpretation of the mobile state as a thermally activated state.

The aim of the present study is to show that molecular-dynamics (MD) simulations, based on classical mechan-

ics, together with realistic potentials can give additional detailed microscopic information and deepen our understanding of H diffusion in bcc metals at high temperatures. The necessary input in a MD simulation is a model for the interatomic interactions. We use the Finnis-Sinclair model for the Nb-Nb interaction[8] and a H-Nb potential proposed by Gillan.[9] The former is semiempirical in nature and invokes some many-atom interactions, present in metallic systems. The latter is given as a simple pair potential with two parameters fitted to the two lowest localized vibrational modes for hydrogen. The obtained numerical value for the diffusion constant well above room temperature is about a factor 2 too large which shows that the potential is reasonable but not accurate. Improvements are certainly feasible and desirable but rather demanding.

We will show that our model reproduces the two key experimental observations: the anomalous Debye-Waller factor and the distinct deviations from simple jump-diffusion behavior. These results are a clear indication that our model for the potential is sufficiently accurate.

The use of a single adiabatic potential-energy surface, describing the interatomic interactions, is based on the Born-Oppenheimer approximation for the separation of the nuclear and electronic degrees of freedom. We have shown in a previous study[10,11] that for light interstitials in metals nonadiabatic effects (excitations of low-lying electron-hole pairs) may become important for the details of the diffusive motion of the interstitial. This effect can be included approximately by adding a friction term and a stochastic force to Newton's equation of motion.[11] We will also consider these effects here but for H in Nb they turned out to be of less importance.

A more critical assumption is the neglect of quantum effects for the hydrogen motion. Unfortunately, there is no powerful molecular-dynamics technique available for solving quantum dynamics in many dimensions. The justification of the neglect of quantum effects has to be accomplished in a more indirect way.

In Sec. II we describe the model for the interaction, both the adiabatic potential-energy surface and how the nonadiabatic corrections are included. Section III gives some information and details on the simulation procedure and in Sec. IV we have collected our results for various quantities, which will be used to establish the validity of our model by comparing directly with experimental data. We also compare our results with the ones obtained using the Chudley-Elliott (CE) model for the diffusive motion.[12] In Sec. V we make use of the exhaustive information contained in the output from the MD simulation and interpret the details of the diffusive motion. Finally, our results and main conclusions are summarized in Sec. VI. Preliminary results of the present study have been presented in Ref. 13.

II. INTERACTION POTENTIAL

A. Adiabatic potential-energy surface

In the molecular-dynamics simulation a potential-energy surface is required. We invoke the usual Born-Oppenheimer approximation and introduce an adiabatic potential-energy surface $E(\{\mathbf{R}\})$. For each configuration $\{\mathbf{R}\}$ of the nuclei the total energy $E(\{\mathbf{R}\})$ of the system is given by electronic ground state for that nuclear configuration.

The Nb-Nb interaction is described by a semiempirical model of Finnis and Sinclair (FS).[8] The physical basis of this model is described in Ref. 8 and a more thorough discussion can be found in Refs. 14 and 15. The energy for the metal is expressed as

$$E_{\mathrm{Nb}}(\{\mathbf{R}\}) = \sum_i F(\rho_i) + \frac{1}{2}\sum_{i\neq j}\phi(R_{ij}), \tag{1}$$

where the indices i and j are used to denote the different Nb atoms. The first term, $F(\rho_i)$, is a many-atom interaction term and is bonding in character. It is written in the form

$$F(\rho_i) = -A\sqrt{\rho_i}\ , \tag{2}$$

where ρ_i is given by a sum over neighboring atoms and the square-root dependence is used to mimic the results of tight-binding theory within the second moment approximation. The parameter ρ_i is then given by the sum of squares of overlap integrals between atom i and its neighbors. The second term, $\phi(R_{ij})$, is a conventional pairwise potential and represents the core-core repulsive interaction between atom i and j separated by a distance $R_{ij} = |\mathbf{R}_i - \mathbf{R}_j|$. Finnis and Sinclair[8] parametrized ρ_i and $\phi(R_{ij})$ according to

$$\rho_i = \sum_j (R_{ij} - d)^2, \quad R_{ij} \leq d \tag{3}$$

and

$$\phi(R_{ij}) = (R_{ij} - c)^2(c_0 + c_1 R_{ij} + c_2 R_{ij}^2), \quad R_{ij} \leq c\ , \tag{4}$$

where the expressions are equal to zero for distances larger than d and c, respectively. All parameters appearing in the above formulas are determined purely empirically by fitting the predicted results of the model to experimental ones for the following bulk properties: lattice constant, cohesive energy, and elastic moduli. For a more detailed description of the procedure see the original paper[8] and for certain deficiencies of the model we refer to a recent paper.[16]

All the sums appearing in Eq. (1) are pairwise sums and applying the FS model requires roughly the same computational effort as compared with a simple pair-potential model. Two deficiencies of the model, however, have already been noticed. The first problem is that the frequency for the short-wavelength phonons given by the model is about 30% too low, resulting in a too low mean phonon frequency. This is corrected by Gillan by multiplying the energy E_{Nb} by a factor 1.9.[9,17] The second problem is that the short-range core-core interactions are too soft and the model suffers from an instability at very small distances.[18] This problem is cured by replacing the

polynomial function $\phi(R_{ij})$ inside the nearest-neighbor distance by an exponential form $B_0+B_1\exp(-R_{ij}/d_{\rm NN})$, where B_0, B_1, and $d_{\rm NN}$ are determined to ensure the continuity of $\phi(R_{ij})$ and its first two derivatives.[9,17]

For the H-Nb interaction we use the same model as Gillan[9,17] and apply the exponential form $Z_0\exp(-R/\alpha)$. The two parameters Z_0 and α are determined by using the two well-separated frequencies for the local vibration of H in Nb: 110 meV and 180 meV.[9,17] The resulting values for Z_0 and α are 25 716 eV and 0.162 Å, respectively. This H-Nb interaction does not reproduce the experimentally determined force-dipole tensor.[17] However, the conventional interpretation of the experiments in terms of static forces has been challenged[3] and we stick to the form suggested by Gillan. Recent calculations by Elsässer *et al.*,[19] based on density functional theory within the local density approximation, indicates, however, a more long-ranged H-Nb interaction and they conclude that the observed force-dipole tensor can be explained by static forces only.

An accurate description of the H–H interaction is not important, since the H concentration we consider is low, $NbH_{0.02}$. Nevertheless, the H–H interaction is assumed to be the same as the Nb–H interaction in order to take into account the repulsion the H atoms experience at short distances.

The above model for NbH_x has been applied extensively by Gillan and co-workers.[9,17,20–22] Both the quantum vibrational states[21] and the diffusive motion of hydrogen[9,17] have been studied and reasonable results have been obtained. Throughout the present study we use exactly the same model as Gillan for the adiabatic potential-energy surface and no further modifications are made.

B. Nonadiabatic corrections

In a previous study[10,11] we have shown that nonadiabatic effects are important for describing the details of H diffusion in Pd, a fcc metal. It is of interest to study the same effect for H in Nb. We will therefore perform two different sets of simulations: One set is denoted by A, where only the adiabatic potential-energy surface described in the previous subsection is used; while in the other set, denoted by B, nonadiabatic corrections are included. These corrections take into account the effects of low-lying electron-hole-pair excitations among the conduction electrons. In this case, not only the adiabatic potential-energy surface but also nonadiabatic ones, close and nearly parallel to it, are relevant. Instead of the single potential-energy surface in case A, we consider in case B a thin potential-energy "shell," including all possible combinations of low-lying electron-hole-pair excitations.

The effects of these excitations can be incorporated in an approximate but reasonable way by introducing a friction term and a stochastic force to the equation of motion, provided the H motion can be treated classically.[11] As a result, Newton's equation of motion is replaced by the equation

$$m_{\rm H}\ddot{\mathbf{R}}_{\rm H} = -\nabla_{\rm H}E(\{\mathbf{R}\}) - m_{\rm H}\overleftrightarrow{\eta}\cdot\dot{\mathbf{R}}_{\rm H} + \mathbf{F}^{\rm st}(t), \qquad (5)$$

where $\nabla_{\rm H}\equiv\partial/\partial\mathbf{R}_{\rm H}$ and $m_{\rm H}$ and $\mathbf{R}_{\rm H}$ are the mass and the position vector for the H atom, respectively. The friction coefficient $\overleftrightarrow{\eta}$ is related to the stochastic force $\mathbf{F}^{\rm st}(t)$ through the fluctuation-dissipation theorem,

$$\langle\mathbf{F}^{\rm st}(t)\mathbf{F}^{\rm st}(t')\rangle = 2m_{\rm H}\overleftrightarrow{\eta}\,k_BT\delta(t-t'), \qquad (6)$$

where k_B is the Boltzmann constant and $\langle\cdots\rangle$ denotes a thermal average. The stochastic force has a white noise spectrum and we assume further that they are Gaussian-type random variables.

In the general case the friction coefficient $\overleftrightarrow{\eta}$ is a tensor and it can be expressed in terms of the density correlation function for the electrons. As a first approximation we consider a hydrogen moving in a homogeneous electron gas and use η values obtained from first-principles calculations for this system.[23] The friction coefficient will then be a scalar quantity and it depends on a single variable, the electron density n. The functional dependence $\eta(n)$, obtained from Ref. 23, is reproduced in Ref. 11. In the case of hydrogen in Pd we used a potential-energy description (the embedded-atom method) which provides a reasonable local electron density for the metal and the density-dependent friction coefficient $\eta(n)$ could be used.[10,11] In the present case that is not the situation and we will use a constant value for η, $\hbar\eta = 2.5$ meV, corresponding to an electron density being equal to the average electron density $\bar{n} = 5.56\times10^{22}$ cm^{-3} in Nb.[24] The local electron density which the H atom experiences, on average, should not be too different from the average electron density in Nb. Our experience from the study of H in Pd is that using the constant value $\eta(\bar{n})$ or a density-dependent $\eta(n)$ gives almost the same results.[10,11] Our main concern here is to study qualitative changes due to the inclusion of the nonadiabatic effects and a more accurate description is not warranted. Technical details on the inclusion of the nonadiabatic effects can be found in Ref. 11.

III. SIMULATION DETAILS

The simulations are carried out for a system with constant total energy, particle number, and volume. It consists of 432 Nb atoms, forming m^3 (with $m = 6$) conventional bcc unit cells, and 8 H atoms, distributed randomly in the metal host. The hydrogen number concentration x is therefore very low, $x = 1.85\%$. We have checked the influence of the system size, varying from $m = 4$ to $m = 7$, and it turns out that $m = 6$ is sufficiently large. The lattice constant is equal to 3.3008 Å and periodic boundary conditions are applied.

Our simulations are performed at two different temperatures $T = 450$ K and $T = 580$ K. The reason for this will become clear in the following section. For each temperature, two cases are considered: with and without including the nonadiabatic effects. The time step in all simulations is equal to 0.5 fs and choosing such a comparatively short time step is because of the rapid motion of the hydrogen atoms. A typical "production run" is of the order $t_{\rm prod} = 100$ ps.

The standard "velocity Verlet" algorithm[25] is used for simulations in set A. When the coupling to electron-hole-pair excitations is included, set B, the algorithm, is extended to include the friction and stochastic forces.[25,11] The trajectories have been measured with respect to the center of mass of the whole system to eliminate the drift of the system introduced by the stochastic forces.

IV. RESULTS

In this section we will establish the validity of our model by comparing directly with experimental data. We will also compare our results with the Chudley-Elliott (CE) model for the diffusive motion.[12,26] In that model it is assumed that the H atom moves from one site to a nearest-neighboring site by random instantaneous jumps and that the jumps are uncorrelated with the vibrational motion at the equilibrium site. We will consider motion on the T sites only and a single parameter enters the model, $\tau_{\rm res}$, the mean residence time at a T site.

A. Atomic site and diffusion path for hydrogen

It is experimentally found that H (D) atoms occupy the interstitial sites with tetrahedral symmetry (T sites) in Nb.[27,28] These sites are shown in Fig. 1. Not all of them are crystallographically equivalent and six nonequivalent T sites are labeled with indices $1,2,\ldots,6$ in Fig. 1.

Our model predicts correctly the atomic sites for H in Nb. Figure 2 shows the potential energy along some directions of particular interest. In calculating the potential energy it is important to take into account the lattice relaxation of the host. It is the relaxed configurations that determine the stable sites and the dominant diffusion paths for hydrogen.[29] Figure 2 shows the results

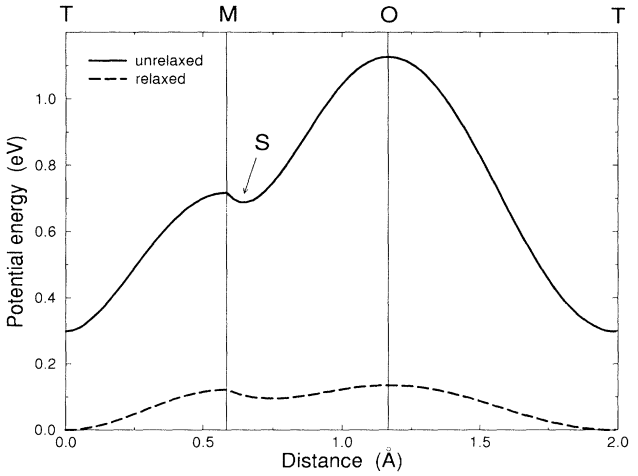

FIG. 2. The relaxed and unrelaxed potential energies with hydrogen located along different directions in the bcc unit cell. The points labeled by T, M, S, and O correspond to the energies when the H atom is located at the tetrahedral T site, the middle point between two T sites, the saddle point located between M and O, and the octahedral site, respectively. The energy is measured with respect to the relaxed energy at the T site.

for both the unrelaxed potential energy, obtained by fixing all Nb atoms at their regular lattice positions; and the relaxed one, where for each given H position the potential energy is minimized with respect to the Nb atom positions. We notice that the configuration with lowest potential energy is the T site. The difference in energy between the unrelaxed and relaxed configurations at the T site, the self-trapping energy, is quite large, 0.30 eV.

The dynamical calculations are consistent with our potential-energy surface. The results from one of the dynamic simulations are shown in Fig. 3, in which the H trajectories have been folded into one bcc unit cell. The figure illustrates the H density distribution in a unit cell.

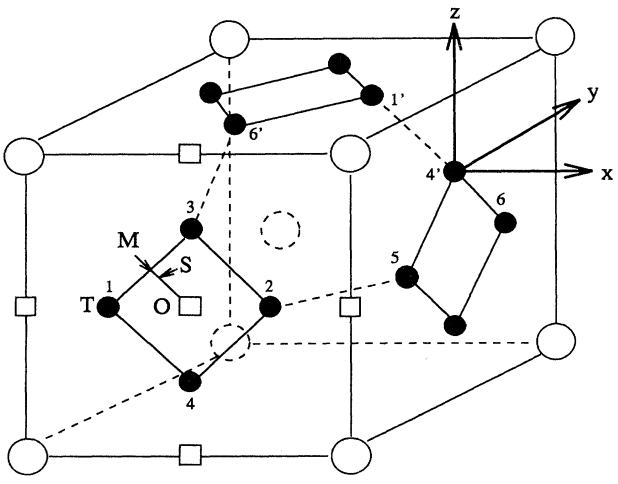

FIG. 1. Unit cell of a bcc lattice. •, tetrahedral interstitial sites (T sites); □, octahedral interstitial sites (O-sites). Six nonequivalent T sites in the cell are labeled by $1,2,\ldots,6$. M denotes the middle point between two T sites and S the saddle point location.

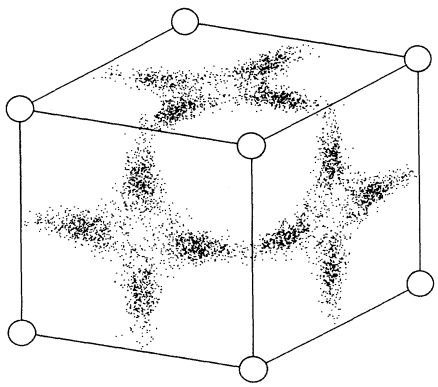

FIG. 3. H locations obtained from the MD simulation. The trajectories for the H atoms have been folded into the bcc unit cell. Dots, the H positions; circles, the equilibrium positions of the host-metal atoms.

Although the results contain also contributions from the diffusive motion, it is clear that the vibrational motion of hydrogen around the T sites dominates. The anisotropic feature of the vibrational amplitude with the stretching along the tetragonal directions is caused by the smaller curvature of the potential well in that direction.

B. Diffusion constant

The diffusivity of hydrogen is directly related to the long-time behavior of the displacement of that particle, $\Delta\mathbf{R}_{\mathrm{H}}(t) \equiv \mathbf{R}_{\mathrm{H}}(t) - \mathbf{R}_{\mathrm{H}}(0)$. For large times the averaged value of the squared displacement increases linearly with time,

$$\langle[\Delta\mathbf{R}_{\mathrm{H}}(t)]^2\rangle = 6D_s t + C, \quad t \text{ large} , \tag{7}$$

where D_s is the so-called tracer-diffusion constant and C is a constant. One example is given in Fig. 4. We deduce the value for D_s from the slope of the linear part of $\langle[\Delta\mathbf{R}_{\mathrm{H}}(t)]^2\rangle$. The same quantity for Nb atoms is also shown in Fig. 4. Clearly, the Nb atoms do not diffuse and $\langle[\Delta\mathbf{R}_{\mathrm{Nb}}(t)]^2\rangle$ approaches a constant value of about 0.034 Å^2. (The oscillations for long times are an artifact caused by the periodic boundary conditions.) This corresponds to the mean squared displacement $\langle u^2_{\mathrm{Nb}}\rangle = 0.0056$ Å^2 for the Nb atoms at 450 K, which is about a factor 1.3 too small compared with the experimental value.[30] Gillan[9,17] "corrected" the potential by Finnis and Sinclair[8] by multiplying the energy by a factor of 1.9 to obtain an accurate mean phonon frequency and it is this "corrected" version we are using. However, the elastic moduli then became too small and in evaluating $\langle u^2_{\mathrm{Nb}}\rangle$ the contributions from the low-frequency phonons are important.

Table I summarizes our results for D_s at two different temperatures and for simulations of both set A and set B. As already noticed by Gillan,[17] the D_s value is slightly higher, about a factor of 2 too large, compared with the experimental result, which is not surprising. In determining the Nb–H interaction only experimental information on the two vibrational frequencies was used and no data on the diffusive motion were taken into account. The experimental data can be well represented by the Arrhenius law $D_0 \exp(-E_a/k_B T)$, with $D_0 = 5.0 \times 10^{-4}$ cm^{-2}s^{-1} and $E_a = 0.106$ eV (for $T > 300$ K).[31] In the same table we also give the mean residence time τ_{res} determined by assuming the Chudley-Elliott (CE) model[12] for the diffusive motion, $\tau_{\mathrm{res}} = a_0^2/48D_s$.

TABLE I. The tracer-diffusion constant D_s at two different temperatures obtained from the simulation without nonadiabatic corrections ($\hbar\eta = 0.0$ meV) and with nonadiabatic corrections included ($\hbar\eta = 2.5$ meV), respectively. T, the simulation temperature; η, the friction coefficient; $t_{\max}$, the length of the production run; τ_{res}, the mean residence time obtained from the relation $\tau_{\mathrm{res}} = a_0^2/48D_s$ [the CE model (Ref. 12)]. The corresponding experimental values are $D_s = 0.33 \times 10^{-4}$ cm^2 s^{-1} and $D_s = 0.60 \times 10^{-4}$ cm^2 s^{-1} at $T = 450$ K and 580 K, respectively (Ref. 31).

T (K)	$\hbar\eta$ (meV)	$t_{\max}$ (ps)	$D_s(10^{-4}$ cm^2 s$^{-1})$	τ_{res}(fs)
450	0.0	100	0.66	345
	2.5	100	0.70	324
580	0.0	100	1.02	223
	2.5	100	1.15	198

To check the seriousness of the deficiency in our model in describing the absolute magnitude of the diffusion constant we have performed simulations at two different temperatures 580 K and 450 K, the higher one being the same as used in the experiment by Dosch *et al.*[3] and the lower one reproducing roughly the same D_s as obtained experimentally at the higher temperature.

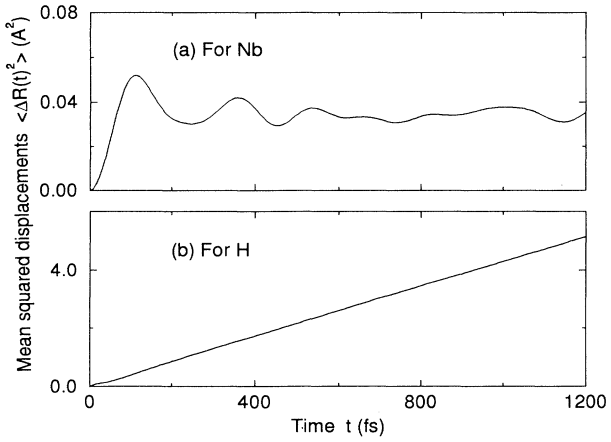

FIG. 4. Mean squared displacements $\langle[\Delta\mathbf{R}(t)]^2\rangle$ for (a) metal atoms and (b) the hydrogen atom, both at T=450 K.

C. Comparison with neutron-scattering results

In incoherent neutron scattering from NbH_x the details of the diffusive motion of hydrogen can be studied by examining the quasielastic peak. Both the q dependence of the linewidth and intensity of this peak show nontrivial behavior. The incoherent intermediate scattering function

$$F_s(\mathbf{q},t) = \langle \exp\{-i\,\mathbf{q}\cdot[\mathbf{R}_{\mathrm{H}}(t) - \mathbf{R}_{\mathrm{H}}(0)]\}\rangle \tag{8}$$

is directly accessible from the MD trajectories (cf. Fig. 8, below) and we have determined both the intensity and width of the quasielastic peak directly from $F_s(\mathbf{q},t)$.

The intensity $I_{\mathrm{QE}}(\mathbf{q})$ is obtained by integrating over a fixed frequency window $[-\omega_0, +\omega_0]$,

$$I_{\mathrm{QE}}(\mathbf{q}) = \int_{-\omega_0}^{\omega_0} d\omega\; S_s(\mathbf{q},\omega) = \frac{2}{\pi}\int_0^{\infty} dt\; \frac{\sin\omega_0 t}{t} F_s(\mathbf{q},t) , \tag{9}$$

where $S_s(\mathbf{q},\omega)$ is the dynamic structure factor, the time-Fourier transform of $F_s(\mathbf{q},t)$. In Fig. 5 we show the result using three different windows together with the experi-

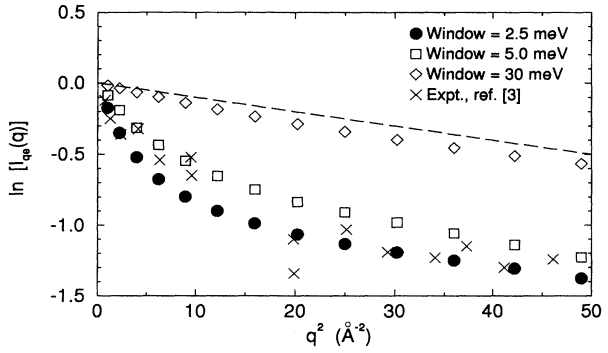

FIG. 5. The logarithm of the integrated intensity of the quasielastic peak, $\ln[I_{\rm QE}(q)]$, as a function of q^2 and with the direction of $\mathbf{q}$ along [100]. The MD data ($\bullet, \Box, \Diamond$) are taken from the simulation at 580 K and with nonadiabatic effects included. Three different energy windows have been used in the integration, as indicated in the figure, and for comparison the experimental data from Ref. 3 are also shown. The dashed line gives the slope corresponding to the contribution from the localized vibrations only.

mental data from Ref. 3. The experimental data have been obtained by fitting the quasielastic peak with a single Lorentzian. In our case, the most narrow window, ± 2.5 meV, corresponds most closely to what is done experimentally (the maximum value for the half width at half maximum in the [100] direction is equal to 1.1 meV at 580 K), but we also show the result using a 2 times larger window, ± 5.0 meV. We notice that our MD results are in qualitative or even semiquantitative agreement with the experimental facts,[3] indicated by crosses in Fig. 5.

In the conventional interpretation of the hydrogen motion in terms of harmonic vibrational motion uncorrelated with the diffusive jumps, which are assumed to be instantaneous compared with the residence time, we would have the relation $\ln[I_{\rm QE}(q)] = -\langle u_H^2\rangle q^2$, where $\langle u_H^2\rangle$ is the mean squared displacement for the vibrational motion.[32] The important finding here is that the slope in a "Debye-Waller plot" ($\ln[I_{\rm QE}(q)]$ versus q^2) changes as function of q and is considerable larger than expected for small q values. By taking only the localized vibrations into account, with energies $\hbar\omega = 100$ meV and $\hbar\omega = 180$ meV, we obtain the averaged value $\langle u_H^2\rangle = 0.01$ Å^2 at 580 K. The corresponding slope is indicated in Fig. 5 by a dashed line. The mean squared displacement also gets a contribution from the so-called band modes, where the hydrogen is moving in phase with the metal atoms. The magnitude of this part is about the same and by including that part the slope would increase by a factor of 2 only.

For large q vectors, $q > 4$ Å^{-1}, the slope is consistent with the one obtained from the localized vibrations only, but for smaller q vectors the slope is considerable larger. This effect has been called the anomalous Debye-Waller factor and it has been observed in several experimental studies.[4–6,3] Several authors[33–35,4] have stressed that the assumption about instantaneous jumps is questionable when the diffusion rate becomes high. The time for the actual jump cannot be neglected compared with the residence time at a site. By taking this effect into account the quasielastic peak is changed considerable.[35] Wakabayashi *et al.*[5] explained the behavior in terms of a temperature-dependent delocalization of the hydrogen. The q dependence of the integrated intensity was fitted with a phenomenological model containing two mean squared displacements, one corresponding to the vibrational motion and one with magnitude comparable to the distance between T sites. With increasing temperature the relative weight of the latter component was found to increase and by assuming an Arrhenius dependence the activation energy 0.1 eV was obtained. Lottner *et al.*[6] made a more careful fit of the line shape of the quasielastic peak. They concluded that for H in Nb no serious deviation from a "normal" Debye-Waller factor occurs and the magnitude of the mean squared displacement was consistent with contributions obtained from the localized and the band modes. However, they had to use more complicated jump-diffusion models in their fitting procedure and they also considered only wave vectors less than 2.4 Å^{-1} for H in Nb. More recently, Dosch *et al.*[3] have made further interpretations of the quasielastic intensity and they stated that a part of the anomalous decrease should be associated with a rapid-diffusion mechanism, on a time scale significantly faster than the conventional long-range diffusion.

We have also used a considerably larger energy window, $\pm$ 30 meV. In this case also the energy range for the band modes [cf. Fig. 9(b), below] is included in the integration and we obtain a "normal" Debye-Waller behavior with the slope roughly corresponding to the localized vibrations only. The key issue will be to characterize correctly the motion which shows up in the energy window $\pm$ 30 meV.

Next we consider the width of the quasielastic peak. Considerable attention has been directed to this quantity and a clear deviation from simple jump-diffusion behavior has been identified.[36,37,34,7,3] We have determined the width by plotting $\ln[F^s(\mathbf{q},t)]$ as a function of time. For long times the slope is linear and the decay is exponential, $\exp[-\Gamma(\mathbf{q})t]$. The decay rate in the time window, 1 ps $< t <$ 2 ps,

$$\Gamma(\mathbf{q}) = -\frac{d}{dt}\ln[F_s(\mathbf{q},t)], \quad 1\ \text{ps} < t < 2\ \text{ps}\ , \qquad (10)$$

is identified with the half width at half maximum of the quasielastic peak. For all data points in Fig. 6 we obtained a clear exponential decay within this time window but for larger q vectors that is not the case.

In Fig. 6 we have added the result using the CE model[12] with jumps between nearest-neighboring sites only. To be consistent we have determined the width in the same way as for the MD data. Only one parameter enters the CE model, the mean residence time $\tau_{\rm res}$, and we show the result for the normalized and dimensionless quantity $\Gamma(q)\tau_{\rm res}$. The same normalization is performed for the MD as well as for the experimental data using the appropriate value for $\tau_{\rm res}$ in each case (cf. Table I). In this way the q dependence of the width is most clearly revealed and by construction all results will agree for suf-

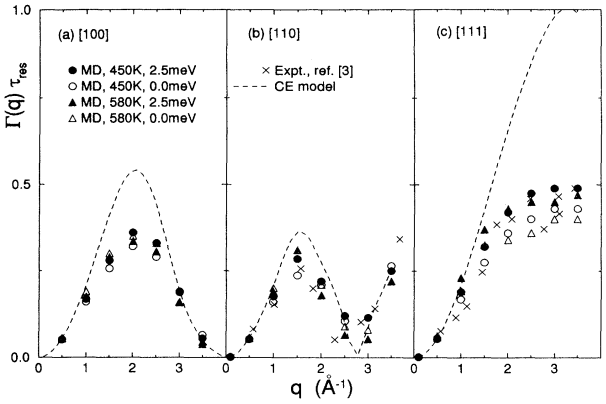

FIG. 6. The half width $\Gamma(q)$ at half maximum of the quasielastic peak in units of $\tau_{\rm res}$. The appropriate numbers for $\tau_{\rm res}$ can be found in Table I and for the experimental data we have used $\tau_{\rm res} = 389$ fs. In the Chudley-Elliott (CE) model the quantity $\Gamma(q)\tau_{\rm res}$ is independent of $\tau_{\rm res}$. The solid symbols show the MD result with nonadiabatic effects included ($\hbar\eta$=2.5 meV) and the open symbols show the corresponding result in the absence of nonadiabatic effects ($\hbar\eta$=0.0 meV). The results along three different directions are shown, as indicated in the figure.

ficiently small q vectors.

The large deviation from the simple jump-diffusion behavior (the CE model), seen particularly in the [111] direction, is reproduced surprisingly well by our MD data. The effect of adding the nonadiabatic effects (the solid symbols in Fig. 6) is not pronounced; the normalized decay of $F_s(\mathbf{q},t)$ only becomes slightly faster for large q vectors.

We conclude that our model reproduces quite well two key experimental observations on the diffusive motion: the anomalous Debye-Waller factor and the strong deviation from simple jump-diffusion behavior.

V. INTERPRETATION

The next step is to make use of the very detailed information contained in the output from the MD simulation. To reveal the details of the diffusive motion we will concentrate on properties that directly show the spatial dependences of the hydrogen motion. In this section we show results only from the simulation at 450 K and with nonadiabatic effects included. The results obtained at the higher temperature, $T = 580$ K, are qualitatively the same. The corresponding mean residence time determined from the diffusion constant is $\tau_{\rm res} = a_0^2/48D_s = 324$ fs, which will be used as the single parameter in the CE model.

A. Van Hove self-correlation function

The first function that has been determined is the Van Hove self-correlation function

$$G_s(\mathbf{r},t) = \langle \delta(\mathbf{r} - [\mathbf{R}_{\rm H}(t) - \mathbf{R}_{\rm H}(0)]) \rangle \ . \qquad (11)$$

In Ref. 13 (Fig. 4) the quantity $4\pi r^2 G_s(\mathbf{r},t)$ is shown, which is equal to the probability at time t to find the hydrogen atom at the distance r from its location at $t = 0$. Three different times are shown, which correspond roughly to the vibrational period, half the mean residence time, and the mean residence time, respectively. The arrows in Fig. 4 in Ref. 13 indicate the distance to the nearest- and to the second-nearest-neighboring T sites, assuming a T site to be located at $r = 0$. The large amplitudes in between the sites show that the hydrogen atom spends considerable time in these regions.

We have also determined the integrated quantity

$$P_0(t) = \int_0^{r_{T-T}} 4\pi r^2 G_s(r,t) dr \ , \qquad (12)$$

where the magnitude for the radius of the sphere is chosen equal to half the distance between T sites, $r_{T-T} = d_{T-T}/2 = 0.58$ Å. Provided the H atom does not spend too much time in the actual jumping process, the "jump phase," we can interpret $P_0(t)$ as the occupancy of the initial site. Assuming the CE model to be valid, the short time decay of $P_0(t)$ is exponential, $\exp(-t/\tau_{\rm res})$, while for longer times the decay is slowed down due to the probability that the H atom can return to the initial site. In Fig. 7 we show our results together with the result obtained from the CE model. Already at $t = 150$ fs the occupancy of the initial site is reduced to 53%. This should be compared with the CE model where the corresponding number is 65%.[38] The difference between these two numbers reveals the existence of a rapid motion where the hydrogen atom is moving between different T sites and which is not accounted for in the CE model.

B. Spatially averaged MD trajectory

The Van Hove self-correlation function $G_s(\mathbf{r},t)$ does not give any direct information on the location of the H

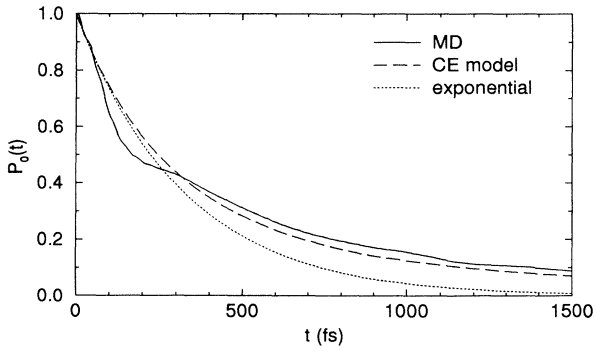

FIG. 7. The Van Hove self-correlation function at 450 K with nonadiabatic effects included. The quantity $P_0(t)$ is shown, which is equal to $G_s(\mathbf{r},t)$ integrated over a sphere with radius $r_{T-T} = 0.58$ Å. The result using the Chudley-Elliott (CE) model is also shown, as well as an exponential with the decay constant $\tau_{\rm res} = 324$ fs.

atom with respect to the metal atoms. We expect hydrogen to move between different T sites but to obtain information on that kind of motion more directly we have to define when the hydrogen atom is located at a particular T site.

We fix the location of the T sites with respect to the undistorted lattice positions of the Nb atoms. The hydrogen atom is then defined to be located at a certain T site whenever it is within the distance r_0 from that site. Hydrogen can then move between different T sites and for simplicity we call this motion "jumps" even if the actual motion is not "jumplike." If the hydrogen exits one sphere of radius r_0 and enters the same sphere without being visiting some other sphere in the mean time ("a large vibration"), this is not counted as a jump. On the other hand, if it exits one sphere and enters another sphere, we count this as a jump and the change of site location is assumed to take place when the hydrogen atom enters the new site. We will show results using $r_0 = 0.3$ Å and $r_0 = 0.4$ Å, both values less than half the distance between two T sites, $r_{T-T} = d_{T-T}/2 = 0.58$ Å. The reason for choosing a sphere radius r_0 which is considerably less than r_{T-T} is that we would like to reduce the contribution from the type of motion that we do not interpret as jumps; for instance, we want to exclude the possibility that if the hydrogen atom only makes a large vibrational type of motion, that is counted as a jump.

In this way we can now introduce a spatially averaged MD trajectory for the hydrogen atom, $\mathbf{R}_{\mathrm{H}}^{d}(t)$, which is equal to the location of the corresponding T site. In contrast to the true MD trajectory $\mathbf{R}_{\mathrm{H}}(t)$ the averaged trajectory $\mathbf{R}_{\mathrm{H}}^{d}(t)$ changes discontinuously. The trajectory $\mathbf{R}_{\mathrm{H}}^{d}(t)$ contains the motion of the hydrogen atom when it is moving between different T sites but not the local vibrational type of motion at the different T sites. We will now make use of these two different trajectories and elucidate the H motion in more detail.

In Fig. 8 we show the intermediate scattering function $F_s(\mathbf{q},t)$ evaluated using both the true MD trajectory $\mathbf{R}_{\mathrm{H}}(t)$ as well as the averaged MD trajectory $\mathbf{R}_{\mathrm{H}}^{d}(t)$. In the same figure we also show the result obtained using the CE model. The long time decay is the same which implies that the half width shown in Fig. 6 would be the same using either $\mathbf{R}_{\mathrm{H}}(t)$ or $\mathbf{R}_{\mathrm{H}}^{d}(t)$. The short time decay, however, is different. Spatially localized motion is more apparent for large wave vectors which explains the more pronounced difference in Fig. 8(b). The substantial decay of $F_s(\mathbf{q},t)$ for times $t < 200$ fs in Fig. 8(b) is caused by vibrational type of motion of the H atom. Oscillations with the period of a few hundred femtoseconds are also visible in Fig. 8(b), which shows that the H atom follows the Nb motion to some extent. We have verified this by artificially changing the time scale for the Nb motion by increasing its mass. The period for the oscillations then becomes longer and is proportional to the square root of the mass.

We have also determined the dynamic structure factor $S_s(\mathbf{q},\omega)$, the time-Fourier transform of the scattering function $F_s(\mathbf{q},t)$, which is directly accessible in neutron-scattering studies. Our results are reproduced in Fig. 9. The spectrum obtained by using the true MD trajectories

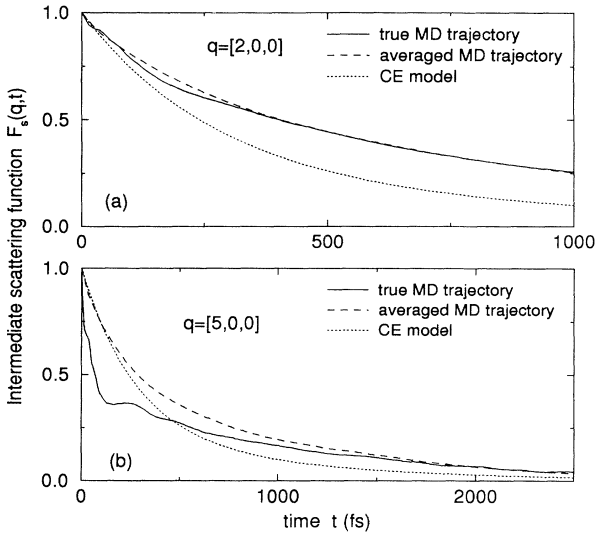

FIG. 8. The intermediate scattering function $F_s(q,t)$ at 450 K with nonadiabatic effects included and for two different wave vectors: (a) $q = [2,0,0]$ Å^{-1} and (b) $q = [5,0,0]$ Å^{-1}. The result from the MD simulation (solid lines) is compared with the Chudley-Elliott (CE) model (dotted lines). The averaged MD trajectory (dashed lines) does not contain the vibrational motion and the parameter value $r_0 = 0.3$ Å has been used (for more details, see the text).

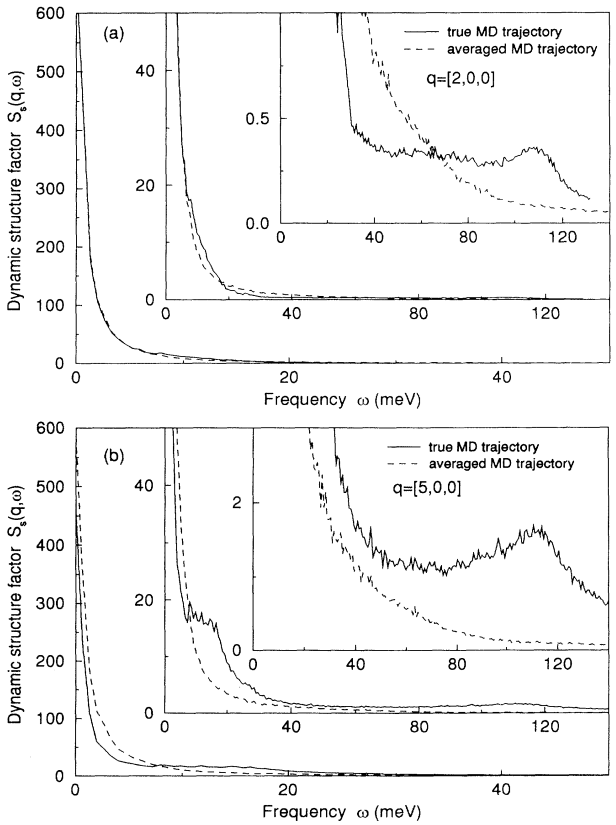

FIG. 9. The dynamic structure factor $S_s(q,\omega)$ for exactly the same conditions as in Fig. 8. Results for two different wave vectors are shown: (a) $q = [2,0,0]$ Å^{-1} and (b) $q = [5,0,0]$ Å^{-1}.

shows a broad peak around 110 meV which corresponds to the localized vibration of the hydrogen atom. There is a also an increased intensity in the frequency range < 20 meV for the larger q vector. If we compare this spectrum with the one obtained using the averaged MD trajectories, we notice that both these features disappear, which directly shows that they are connected to spatially localized motion. The frequency range < 20 meV coincides with the phonon spectrum for the metal host[39] and this feature in the spectrum corresponds to the so-called band modes where the hydrogen atom is vibrating in phase with the surrounding metal atoms.

The identity $F^s(\mathbf{q}, t = 0) \equiv 1$ implies that the total intensity obtained from the two different spectra is the same. For the averaged trajectory the intensity for the vibrational motion disappears but that intensity has to reappear at other places. The quasielastic peak becomes larger but the half width at half maximum of that peak is the same. Therefore one has to be a little careful and not compare the absolute intensities directly.

C. Residence-time distribution

The trajectory $\mathbf{R}_{\mathrm{H}}^d(t)$ contains information on the residence time at the different sites. We define the residence time as the time difference between the moment when the H atom first enters a site until it enters another site. In Fig. 10 we show the result for the distribution of the residence times using two different values for r_0: 0.4 Å and 0.3 Å. The integral of the distributions gives the total number of jumps which are found to be 4230 and 3519, respectively. The time extension of the simulation is $t_{\max}$=125 ps and we have n_H=8 H atoms in the simulation cell. Assuming the CE model to be valid we would have an exponential distribution for the residence times, $\exp(-t/\tau_{\mathrm{res}})$, and the total number of jumps would have been $N_{\mathrm{CE}} = n_H t_{\max}/\tau_{\mathrm{res}} = 3086$. This is less than found in the simulation and for comparison we also show the result from the CE model in Fig. 10, properly normalized.

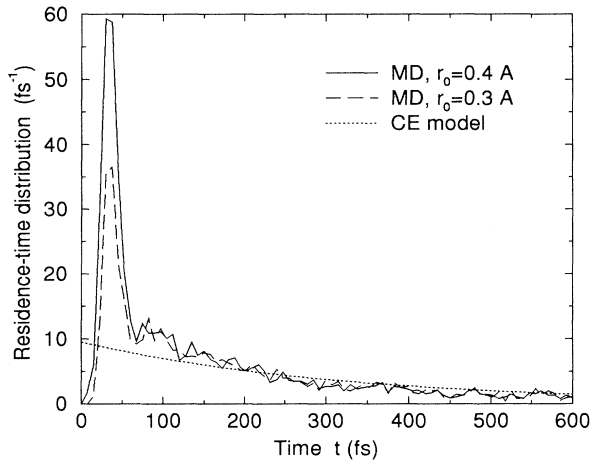

FIG. 10. The distribution of the residence times for the hydrogen to be located at a T site, taken from the simulation at 450 K and with nonadiabatic effects included. The precise definition of the residence time is given in the text and we have used two different values for the parameter r_0, as indicated in the figure. The MD data are compared with the Chudley-Elliott (CE) model using τ_{res}=324 fs and the appropriate number of jumps.

The distribution, found in the MD simulation, is composed of two distinct contributions: one narrow component with a short residence time of the order 35 fs and one broad component extending to longer times. The former corresponds to the "flight" motion during which a H atom moves through a sphere of radius r_0 surrounding a T site, instead of being trapped therein. The magnitude of the narrow component depends on the chosen value for r_0; it becomes larger for larger values of r_0. The reason is that more portions of the trajectories will be counted as jumps. We can compare the time scale 35 fs with the time it takes a H atom with thermal velocity to move from one T site to another which is equal to $d_{T-T}/\sqrt{k_B T/m_{\mathrm{H}}} =$ 60 fs at T = 450 K.

The latter contribution in the residence-time distribution can roughly be approximated with an exponential decay. This contribution is found to be independent of the chosen value for r_0, in contrast to the narrow component. The H atom is trapped within a T site and vibrates locally which implies that the residence time will be independent on the particular value for r_0. For short times the decay is faster compared with longer times. A fit in the time window 60 fs $<$ t $<$ 300 fs leads to the typical decay time 160 fs while in the time window 300 fs $<$ t $<$ 600 fs the decay time is closer to 300 fs. For longer times the decay is even slower but due to the statistical uncertainties it is difficult to estimate a numerical value. These numbers should be compared with the mean residence time derived from the diffusion constant, $\tau_{\mathrm{res}} = a_0^2/48D_s$ = 324 fs, and we find that the decay rate in the time window 60 fs $< t <$ 300 fs is faster than expected from a simplified description.

We have also determined the mean residence time. The following numbers are obtained: 229 fs and 275 fs for r_0 = 0.4 Å and 0.3 Å, respectively. The difference is due to the different magnitudes of the narrow component. By removing that peak we obtain the value 296 fs. This is done by artificially assigning the number 12 to the distribution function in the time window $20 < t < 50$ fs. The value 296 fs is rather close the the CE value $\tau_{\mathrm{res}} = a_0^2/48D_s = 324$ fs.

Next we will consider the correlation in direction between consecutive jumps and decompose the residence-time distribution into different cases.

D. Jump-angle distribution

Two consecutive jumps define a jump angle θ. In Fig. 11 we show the most common cases, found in the simulation. Cases (a)–(c) correspond to two consecutive nearest-neighboring jumps and in cases d and e a nearest-neighboring jump is followed by a second-nearest-neighboring jump. The last two angles are also obtained if the second-nearest-neighboring-jump is followed by the

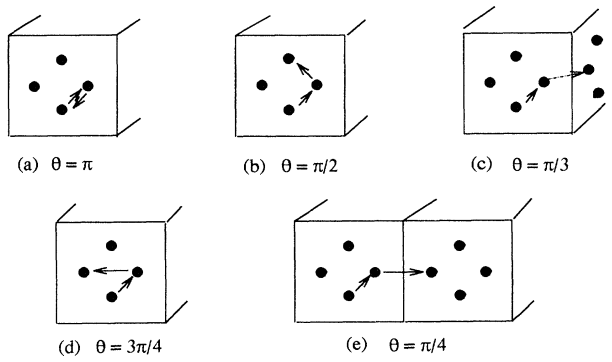

FIG. 11. Illustration of different jump angles.

nearest-neighboring jump. In the simulation we have also found a few cases with $\theta = 0$. In the CE model only the jump angles in cases (a)–(c) are present and the probability for case (c) is twice as large as for the other two.

In Fig. 12 we show the occurrence of different jump angles obtained from the simulation using $r_0 = 0.4$ Å. For comparison we also show in Fig. 13 the corresponding result using the CE model. The CE model gives a rather poor description of the true behavior. In particular, we find a high probability of direct backward jumps and a substantial contribution of second-nearest-neighboring jumps.

In order to extract more information we have also divided the jump angles into three different categories, depending on the magnitude of the residence time at the site between the two consecutive jumps. Three time intervals have been considered: $t < 60$ fs, 60 fs $< t <$ 300 fs, and $t >$ 300 fs. For comparison we have made the same division for the CE model in Fig. 13.

We obtain a large portion with residence times shorter than 60 fs, in direct accordance with the distribution

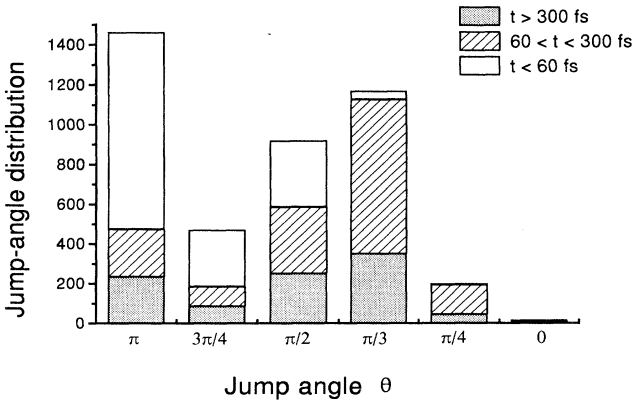

FIG. 12. The jump-angle distribution, taken from the simulation at 450 K and with nonadiabatic effects included. The parameter value r_0=0.4 Å is used and the different jump angles are illustrated in Fig. 11. For a given θ value the distribution is divided into three different categories: $0< t <$60 fs, 60 fs$< t <$300 fs, and $t >$300 f, depending on the magnitude of the residence time t at the site between the two consecutive jumps which define the jump angle.

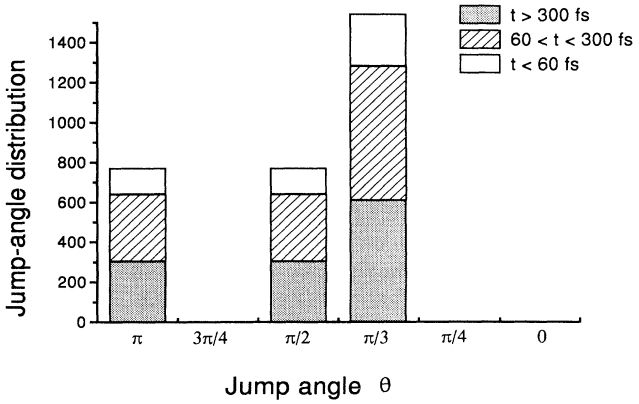

FIG. 13. The same as in Fig. 12 but assuming the Chudley-Elliott model to be valid with an exponential residence-time distribution (τ_{res}=324 fs) and with uncorrelated jumps to nearest-neighboring sites only.

function in Fig. 10. The difference between the MD data and the CE model is manifest. The cases with short residence times are found predominantly for jump angles specified by cases (a), (b), and (d). These angles define the so-called $4T$ configuration[3] and we can directly conclude that this rapid motion, with residence times less than 60 fs, is confined to that type of configuration. The $6T$ or $3T$ configuration,[3] which involvess case (c) ($\theta = \pi/3$) only, is considerably less involved.[40] Many of the above events correspond to the fact that the H atom vibrates locally around one T site, makes a large, but short-in-time detour to a nearest-neighboring T site, and then reenters back to the original T site [cf. Fig. 14(b)]. Others correspond to a more complicated jump with large detours to nearby T sites [cf. Figs 14(c) and 14(d)]. These kinds of motions give rise to an anomalous q dependence of the intensity of the quasielastic peak,[5] a fast initial decay followed by a slower decay for larger q values (cf. Fig. 5).

For longer times, t > 60 fs, the occurrence of jump angles defined by cases (a)–(c) is roughly the same as within the CE model with slightly fewer for case (a), $\theta=\pi$. In the time window 60 fs $< t <$ 300 fs jumps with $\theta=\pi/3$, case (c), is somewhat more likely compared with cases (a) and (b). Substantial contributions are also obtained from second-nearest-neighboring jumps [cases (d) and (e)] which are absent in the CE model. We have determined the total number of nearest- and second-nearest-neighboring jumps and about 10% is found to be of the latter category. More precisely, for $r_0 = 0.4$ Å we obtained 3832 nearest-neighboring jumps and 398 second-nearest-neighboring jumps while for $r_0 = 0.3$ Å the corresponding numbers are 3179 and 340, respectively. One should also have in mind that a more complicated event, as, for instance, the one shown in Fig. 14(c), is here counted *not* as a single second-nearest-neighboring jump but as two nearest-neighboring jumps (in that particular case). The conclusion is that the diffusive motion is considerably more complicated than within the CE model. This is apparent in the q dependence of the width of the quasielastic peak (cf. Fig. 6).

E. Trajectories

In Fig. 14 we have collected some typical H trajectories, projected onto the (100) surface of the bcc unit cell. Each panel shows the time evolution of the H position for 500 fs. The solid circles denote the lattice positions of the Nb atoms and the open circles the positions of the T sites assuming the parameter value r_0=0.4 Å. In (a) the H atom makes a "diffusive" jump between two nearest-neighboring T sites while in (b) it vibrates locally and only makes a large detour to a nearest-neighboring T site. The motion in (b) will be counted as two nearest-neighboring jumps with angle $\theta=\pi$ (cf. Fig. 11) and the residence time at the site between the two consecutive jumps is very short, of the order 20 fs. In (c) and (d) the H atom performs a more complicated motion. The motion in (c) will be counted as two nearest-neighboring jumps with angle $\theta=\pi/2$ and residence time 100 fs. In (d) a nearest-neighboring jump is followed by a second-nearest-neighboring jump, the jump angle is $\theta=3\pi/4$, and the residence time 30 fs.

The trajectories in Fig. 14 are shown for illustrative purpose only. To get a quantitative measure of the relative importance of different kinds of motion statistically averaged quantities, as presented in the previous subsections, have to be determined.

F. Potential-energy surfaces

We have also tried to obtain some information on the probability for the occurrence of different configurations

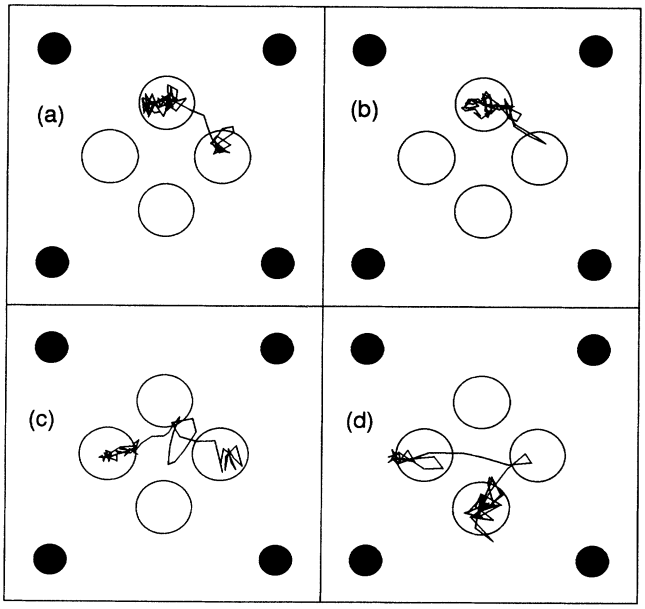

FIG. 14. Illustration of different kinds of H trajectories, projected onto the (100) surface of the bcc unit cell. Each panel shows the time evolution of the H position for 500 fs. The solid circles denote the lattice positions of Nb atoms and the open circles the positions of the T sites assuming the parameter value r_0=0.4 Å.

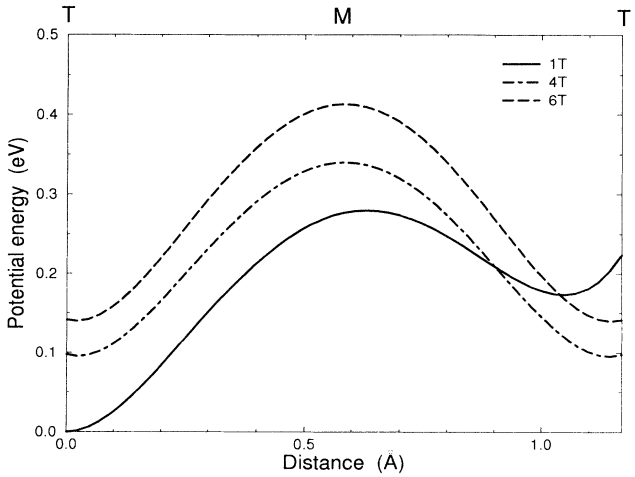

FIG. 15. The potential energy as function of the H position along the straight line from one T site to another T site (e.g., positions 2 and 3 in Fig. 1). The Nb positions are kept fixed in three different arrangements, denoted as $1T$, $4T$, and $6T$. $1T$ corresponds to the distortion caused by a fixed H atom at one T site (position 2) while $4T$ and $6T$ correspond to a "delocalized" H atom, located at $4T$ and $6T$ sites, respectively. For more details, see the text.

by investigating the potential-energy surface. In Fig. 2 we have shown the potential energy for the total system as function of the hydrogen position. For each position of the hydrogen atom the system is allowed to relax to the configuration with minimum potential energy. Another function can be obtained by first relaxing the system in the presence of a fixed hydrogen atom, and then determine the potential energy as function of the hydrogen position with frozen configuration for the Nb atoms.

We have considered three such cases; denoted as $1T$, $4T$, and $6T$. The $1T$ arrangement has been derived by first locating the hydrogen atom at one T site (position 2 in Fig. 1). The system is then allowed to relax and with frozen Nb positions the potential energy as function of the H position is obtained and shown in Fig. 15 (solid line).[44]

The $4T$ arrangement corresponds to the situation where the influence of the hydrogen atom is divided equally between four different T sites (positions 2, 4, 1, and 3 in Fig. 1). Technically this is done by locating four "H atoms" at the different T sites and then reducing the H-Nb interaction strength by a factor of 4. In this way we obtain a distorted configuration which is symmetric with respect to these four different T sites. In the same way, the $6T$ arrangement is obtained by dividing the influence of the hydrogen atom equally on six T sites; denoted by 2, 3, 6′, 1′, 4′, and 5 in Fig. 1. Figure 15 shows the potential energy obtained by moving the hydrogen atom from one T site (position 2) to the nearest-neighboring T site (position 3) in a straight line. In all cases the Nb configurations are frozen.

First we notice that the energy required to create a $4T$ arrangement, with the hydrogen located at one T site equal to ΔE=0.10 eV. At an elevated temperature there

is therefore a finite probability to obtain such a fluctuation. The energy barrier, however, in that configuration is substantial and the configuration is not at all "flat." We find no direct evidence for the formation of a "cage," a region extended over several T sites with roughly constant potential energy for the H atom, where that atom could move rather freely and rapidly back and forth several times. The motion is highly cooperative in nature and only from the time-dependent MD calculation can the proper behavior be deduced.

VI. SUMMARY AND CONCLUSIONS

In this paper results from a molecular-dynamics (MD) simulation of H diffusion in Nb have been presented. The system consists of 432 Nb atoms and 8 H atoms, giving the hydrogen number concentration $x = 0.0185$. Two different temperatures are considered: T= 450 K and T = 580 K. For the interatomic interactions we have used a potential-energy surface proposed by Finnis and Sinclair,[8] and Gillan.[9]

Our model reproduces quite well two key experimental observations on the quasielastic peak: the distinct deviation from simple jump-diffusion behavior for the wave-vector dependence of the width of the peak and the anomalous wave-vector dependence of the integrated intensity of the same peak, the Debye-Waller factor. We also identify in the spectrum localized vibrational modes and band modes, where the H atom is moving in phase with the metal atoms. These findings confirm that our rather crude model for the potential-energy surface is sufficiently accurate for our purposes.

To reveal the details of the hydrogen motion we have considered quantities that directly describe the time dependence of the spatial location of the H atom with respect to the surrounding metal atoms. We define the H atom to be located at a particular T site whenever it is within the distance r_0 from that site, with r_0 in the range $0.3\ \text{Å} < r_0 < 0.4\ \text{Å}$. Both the distribution of the residence times at the T sites and the correlation character among consecutive jumps have been determined.

We find that the residence-time distribution is composed of two distinct contributions: one narrow component with a short residence time of the order 35 fs and one broad component with roughly exponential decay.

The former corresponds to the fact that the H atom moves rapidly through a T site and one may interpret this as the jump phase. This rapid motion, with short residence time, is found predominantly for jump angles specified by cases (a), (b), and (d) in Fig. 12, which define the so-called $4T$ configuration. However, we have found no evidence for the formation of a long-lived "cage" extended over a $4T$ configuration where the H atom could move rapidly and repeatedly back and forth. Many of the rapid events are simply motions where the H atom vibrates locally, makes a large detour, and then reenters back to the original site [cf. Fig. 14(b)]. These findings are quite consistent with the physical picture proposed by Wakabayashi *et al.*[5] in order to explain the anomalous Debye-Waller factor. We have also identified this with the "rapid local diffusion,"[13] discussed recently by Dosch *et al.*[3]

The broad component in the residence-time distribution is found to be independent of the chosen value for r_0, in contrast to the narrow component. The typical decay time is found to be of the order 160 fs and 300 fs in the time intervals 60 fs $< t <$ 300 fs and 300 fs $< t <$ 600 fs, respectively. This should be compared with the mean residence time derived from the diffusion constant, $\tau_{\text{res}} = a_0^2/48D_s = 324$ fs, and, therefore, the decay rate in the time window 60 fs $< t <$ 300 fs is faster than expected from a simplified description.

A conclusion one can draw from our simulation results is that the diffusive motion of H at high temperatures in bcc metals is quite complicated. If we view the type of motions shown in Figs. 14(c) and 14(d) as single-jump events, it is clear that in order to characterize that motion correctly the time spent and the spatial excursion performed in the jump phase cannot be neglected. We also find substantial contributions of second-nearest-neighboring jumps and we stress that the division between nearest- and second-nearest-neighboring jumps is ambiguous. The diffusive and the vibrational motion of the H atom cannot be clearly separated, which implies that the description of the diffusive motion in terms of simplified phenomenological models becomes difficult.

The quantum aspects of the hydrogen motion have been neglected. Using the path-integral simulation technique Gillan[17] has shown that around 500 K the hydrogen atom is rather well localized in space and it is therefore reasonable to assume that the *dynamics* of the hydrogen motion can be approximated by classical mechanics. The discrete nature of the energy levels would more show up as an implicit temperature- and isotope-dependent shift in the potential-energy surface. These effects are not negligible even at 500 K (Ref. 45) and care has to be taken if data from first-principle calculations of the potential are used as input in a MD simulation based on classical mechanics. The fact that our results reproduce experimental observations quite well provides a further indication of the credibility of assuming classical dynamics at the present temperatures.

ACKNOWLEDGMENTS

Financial support from the Swedish Natural Science Research Council (NFR) and the Swedish Board for Industrial and Technical Development (NUTEK) together with allocation of computer time at the UNICC facilities at Chalmers University of Technology are gratefully acknowledged. We would also like to thank Professor H. Dosch, Professor A. Sjölander, Professor A. M. Stoneham, and Professor H. Wipf for valuable comments.

* Electronic address: yinggang@aztec.fi.ameslab.gov
† Electronic address: wahnstrom@fy.chalmers.se

[1] *Hydrogen in Metals I, Basic Properties*, Topics in Applied Physics, Vol. 28, edited by G. Alefeld and J. Völkl (Springer-Verlag, Berlin, 1978).
[2] Y. Fukai, *The Metal-Hydrogen System, Basic Bulk Properties* (Springer-Verlag, Berlin, 1993).
[3] H. Dosch, F. Schmid, P. Wiethoff, and J. Peisl, Phys. Rev. B **46**, 55 (1992).
[4] W. Gissler, B. Jay, R. Rubin, and L. A. Vinhas, Phys. Lett. **43A**, 279 (1973).
[5] N. Wakabayashi, B. Alefeld, K. W. Kehr, and T. Springer, Solid State Commun. **15**, 503 (1974).
[6] V. Lottner, A. Heim, and T. Springer, Z. Phys. B **32**, 157 (1979).
[7] V. Lottner, J. W. Haus, A. Heim, and K. W. Kehr, J. Phys. Chem. Solids **40**, 557 (1979).
[8] M. W. Finnis and J. E. Sinclair, Philos. Mag. A **50**, 45 (1984).
[9] M. J. Gillan, Phys. Rev. Lett. **58**, 563 (1987).
[10] Y. Li and G. Wahnström, Phys. Rev. Lett. **68**, 3444 (1992).
[11] Y. Li and G. Wahnström, Phys. Rev. B **46**, 14 528 (1992).
[12] C. T. Chudley and R. J. Elliott, Proc. Phys. Soc. London **77**, 353 (1961).
[13] G. Wahnström and Y. Li, Phys. Rev. Lett. **71**, 1031 (1993).
[14] M. W. Finnis, A. T. Paxton, D. G. Pettifor, A. P. Sutton, and Y. Ohta, Philos. Mag. A **58**, 143 (1988).
[15] A. E. Carlsson, in *Solid State Physics*, Vol. 43, edited by H. Ehrenreich and D. Turnbull (Academic, New York, 1990).
[16] G. H. Campbell *et al.*, Phys. Rev. Lett. **70**, 449 (1993).
[17] M. J. Gillan, Philos. Mag. A **58**, 143 (1988).
[18] G. J. Ackland and R. Thetford, Philos. Mag. A **56**, 15 (1987).
[19] C. Elsässer, M. Fähnle, L. Schimmele, C. T. Chan, and K. M. Ho, Phys. Rev. B **50**, 5155 (1994).
[20] F. Christodoulos and M. J. Gillan, Philos. Mag. B **63**, 641 (1991).
[21] F. Christodoulos and M. J. Gillan, J. Phys. Condens. Matter **3**, 9429 (1991).
[22] M. J. Gillan and F. Christodoulos, Int. J. Mod. Phys. C **4**, 287 (1993).
[23] M. J. Puska and R. M. Nieminen, Phys. Rev. B **27**, 6121 (1983).
[24] N. W. Ashcroft and N. D. Mermin, *Solid State Physics* (Holt, Rinehart and Winston, New York, 1976).
[25] M. P. Allen and D. J. Tildesley, *Computer Simulation of Liquids* (Oxford, New York, 1987).
[26] J. M. Rowe, Kurt Sköld, H. E. Flotow, and J. J. Rush, J. Phys. Chem. Solids, **32**, 41 (1971).
[27] H.-D. Carstanjen, Phys. Status Solidi (A) **59**, 11 (1980).
[28] E. Yagi, S. Nakamura, T. Kobayashi, K. Watanabe, and Y. Fukai, J. Phys. Soc. Jpn. **54**, 1855 (1985).
[29] U. Engberg, Y. Li, and G. Wahnström, J. Phys. Condens. Matter **5**, 5543 (1993).
[30] H. Behr, H. M. Keppler, H. Metzger, and J. Peisl, Z. Phys. B **55**, 95 (1984).
[31] J. Völkl and G. Alefeld, in Ref. 1.
[32] K. Sköld, in Ref. 1.
[33] L. A. de Graaf, J. J. Rush, H. E. Flotow, and J. M. Rowe, J. Chem. Phys. **56**, 4574 (1972).
[34] N. Stump, W. Gissler, and R. Rubin, Phys. Status Solidi B **54**, 295 (1972).
[35] W. Gissler and N. Stump, Physica **65**, 109 (1973).
[36] W. Gissler, G. Alefeld, and T. Springer, J. Phys. Chem. Solids **31**, 2361 (1970).
[37] G. Kistner, R. Rubin, and I. Sosnowska, Phys. Rev. Lett. **27**, 1576 (1971).
[38] In Ref. 13 the incorrect number 85% was given for the CE model. The correct value is 61% (at $t = 170$ fs).
[39] B. M. Powell, P. Martel, and A. D. B. Woods, Can. J. Phys. **55**, 1601 (1977).
[40] In our case the H motion is treated purely classically and the "delocalization" of the H atom over several T sites is not the same as the delocalization of quantum mechanical origin, discussed, e.g., in Refs. 41–43.
[41] A. M. Stoneham, Ber. Bunsenges. Phys. Chem. **76**, 816 (1972).
[42] J. Buchholz, J. Völkl, and G. Alefeld, Phys. Rev. Lett. **30**, 318 (1973).
[43] H. K. Birnbaum and C. P. Flynn, Phys. Rev. Lett. **37**, 25 (1976).
[44] This function can be used to approximately determine the vibrational frequencies for H in Nb (cf. Ref. 21).
[45] B. von Sydow, G. Wahnström, and Y. Li, J. Alloys Compounds (to be published).